Nanoscale

PAPER

View Article Online
View Journal | View Issue

Cite this: *Nanoscale*, 2014, **6**, 5807

Localized plasmon assisted structured illumination microscopy for wide-field high-speed dispersion-independent super resolution imaging

Joseph Louis Ponsetto, Feifei Wei and Zhaowei Liu*

Received 23rd January 2014
Accepted 3rd April 2014

DOI: 10.1039/c4nr00443d

www.rsc.org/nanoscale

A new super resolution imaging method, *i.e.* Localized Plasmon assisted Structured Illumination Microscopy (LPSIM), is proposed. LPSIM uses an array of localized plasmonic antennas to provide dynamically tunable near-field excitations resulting in finely structured illumination patterns, independent of any propagating surface plasmon dispersion limitations. The illumination pattern feature sizes are limited only by the antenna geometry, and a far-field image resolved far beyond the diffraction limit is obtained. This approach maintains a wide field of view and the capacity for a high frame-rate. The recovered images for various classes of objects are presented, demonstrating a significant resolution improvement over existing methods.

Introduction

The use of optical microscopes has had a profound impact in the field of biology for many decades. Visible light is generally safe and will not damage a living sample. As biologists have delved deeper into the study of living structures, however, the demand has increased for live images with resolution on the scale of cellular organelles and beyond. Unfortunately, the wave-particle duality of light places a fundamental limit on the spatial resolution achievable for a given illumination wavelength. This is known as the Abbe diffraction limit, and states that the smallest resolvable distance d between two objects is about $d = \lambda/2\mathrm{NA}$, where NA is the numerical aperture of the objective, and λ is the wavelength of the light illuminating the sample. This leads to a maximum imaging resolution of approximately 200 nm for visible light. High-energy, short-wavelength probes such as X-rays or electrons can indeed provide additional imaging detail, but these methods are inherently harmful to most organic samples.

With the increasing demand for high resolution using visible light, many novel microscopy techniques have been proposed and shown experimentally in recent years. These methods include single molecule localization,[1,2] stimulated emission depletion microscopy (STED),[3,4] near-field scanning optical microscopy (NSOM),[5,6] the far-field superlens (FSL),[7–9] the hyperlens,[10,11] the metamaterial immersion lens (MIL),[12] structured illumination microscopy (SIM),[13–17] plasmonic structured illumination microscopy (PSIM),[18] and others.[19,20] Although these methods have found successful application in laboratories and as commercial equipment, each has its respective limitations.

Department of Electrical and Computer Engineering University of California, San Diego 9500 Gilman Drive, La Jolla, CA 92093-0406, USA. E-mail: zhaowei@ucsd.edu

For high-resolution, high-speed, *in vivo* imaging, SIM has proven especially useful. The optical transfer function (OTF) of a standard, diffraction-limited epifluorescence microscopy setup can be represented by a circle with a radius determined by the cutoff frequency $\boldsymbol{k}_{\mathrm{cutoff}} \cong 2\mathrm{NA}/\lambda$ (see the central circles in Fig. 1). SIM uses Moiré fringes to bring high-frequency information into the detectable regime, thus improving the image

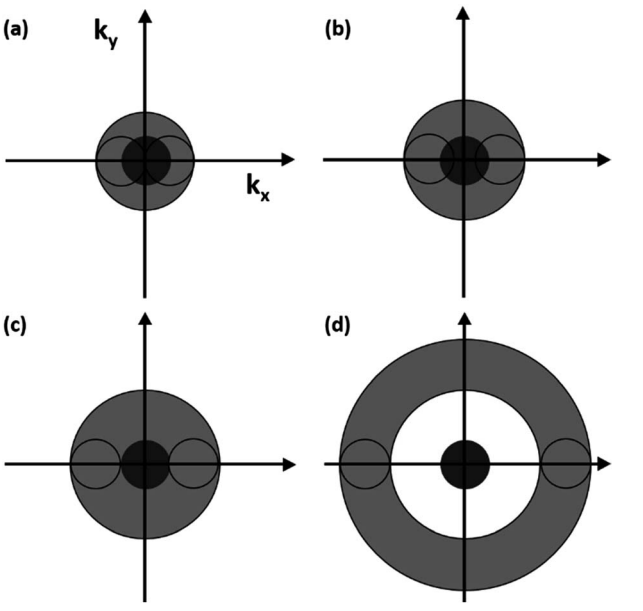

Fig. 1 k-space illustration of resolving power: The dark central circle represents the spatial frequencies detectable with a diffraction-limited imaging setup. (a) OTF of the SIM technique. (b) PSIM OTF. (c and d) Two potential LPSIM schemes using excitation patterns with large k-vectors, dramatically enhancing resolving power.

resolution.[21] This process can be described in real space and frequency space by the following equations,

$$m(\boldsymbol{r}, \varphi) = \{o(\boldsymbol{r})[1 + \cos(\boldsymbol{K}x + \varphi)]\} \times p(\boldsymbol{r}) \quad (1)$$

$$M(\boldsymbol{k}, \varphi) = P(\boldsymbol{k})\left\{O(\boldsymbol{k}) + \frac{1}{2}\left[e^{i\varphi}O(\boldsymbol{k} + \boldsymbol{K}) + e^{-i\varphi}O(\boldsymbol{k} - \boldsymbol{K})\right]\right\} \quad (2)$$

where m is the recorded image, o is the actual object, p is the point spread function (PSF) of the microscope, and $1 + \cos(\boldsymbol{K}x + \varphi)$ represents an example structured illumination pattern, with spatial frequency $\boldsymbol{K}$ and phase φ. As can be seen from the above equations, this imaging process provides information outside the standard OTF. Several sub-images are collected with different pattern phases and orientations, and a full super-resolved image is reconstructed. This method has proven remarkably successful, although its illumination pattern is still inherently limited by diffraction. This leads to a two-fold resolution improvement (Fig. 1a) compared to conventional epifluorescence microscopy, with a best-case resolution of approximately 100 nm for visible illumination wavelengths. Several new methods have been proposed, such as saturated structured illumination microscopy (SSIM), and random speckle illumination.[22] However, these methods have significant drawbacks including fluorescent bleaching (SSIM), slow imaging speed, and a high number of sub-images required.

In this letter, we propose a novel, deeply sub-diffraction optical imaging technique called localized plasmon assisted structured illumination microscopy (LPSIM), which uses localized plasmons (LPs) generated on an antenna array in concert with reconstruction methods based on known illumination patterns to significantly improve resolving power (two potential OTFs shown in Fig. 1c and d). We will describe in detail the physical principles of the LPSIM, and then show an exemplary numerical demonstration of the performance of the proposed method. Advantages and disadvantages of this technique will also be discussed.

Localized plasmon resonances are physically understood as collective electron charge oscillations in metallic structures, excited by incident electromagnetic radiation.[23] These phenomena have been studied at length, and have found practical use in a wide range of fields.[24–30] With recent advances in nanoscale fabrication techniques, controlling electric fields at nanoscale has become a valuable tool. Because LPs are fundamentally bound to the metal–dielectric interfaces they inhabit, their size is determined primarily by the geometry of the interface. LPSIM takes advantage of this characteristic, utilizing plasmonic excitations on a 2D array of LP antennas, which serve as structured illumination patterns. These patterns, unlike those of SIM or PSIM, can have almost arbitrary spatial frequency, so the spatial resolution obtainable with this method is not fundamentally limited by free-space or propagating surface plasmon polariton dispersion relations (see Fig. 2g). This allows us to collect $\boldsymbol{k}$-space information from arbitrary regions based on the LP antenna array design. In this letter, we place our LPSIM $\boldsymbol{k}$-ring as shown in Fig. 1c, for a 3× resolution improvement over standard microscopy.

Our antenna design and illumination scheme is described in the Experimental section, and is shown in Fig. 2. The silver

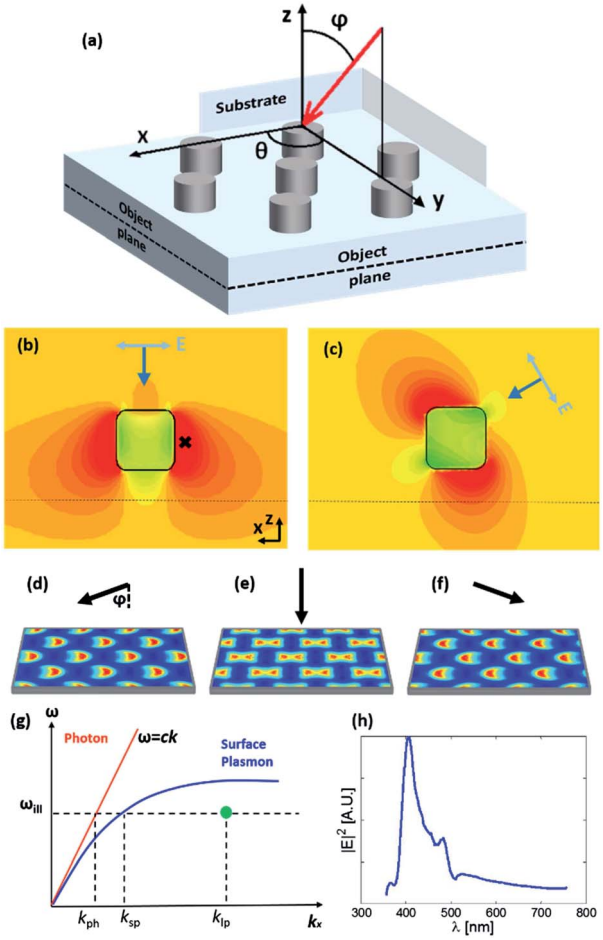

Fig. 2 Proposed imaging scheme: (a) schematic for LPSIM pattern translation. The red arrow represents p-polarized laser light, directed towards the plasmonic substrate at varying angles to create near-field excitation patterns a short distance behind the antennas, in the object plane. (b and c) Field strength around a nanodisc excited by laser light at incident angles of $\theta = 0°$, $\varphi = 0°$ and 60°, respectively. (d–f) Object plane patterns for incident angles $\theta = 0°$ and $\varphi = 60°$, 0°, −60° respectively, as used in reconstruction. (g) Dispersion advantage of LPSIM over existing methods. SIM and PSIM are limited by the red and blue dispersion curves, respectively. For LPSIM, the green dot shown is determined only by the antenna geometry. (h) Electric field magnitude at a fixed position (see the "x" in part (b)) for a single nanodisc under normally-incident illumination showing resonant behavior.

nano-antennas are 60 nm in diameter with a one to one aspect ratio. They are spaced 150 nm apart (center to center). The hexagonal array structure (see schematic in Fig. 2a) has 3-fold rotational symmetry, allowing us to scan our plasmonic pattern in three orientations to collect the full Fourier information. Changes to the plasmonic pattern were controlled by the incident illumination angle, and resulted in tunable excitations, as shown in Fig. 2b–f. Despite our dispersion-independent excitation patterns, the incident wavelength matters for two reasons. For one, because the standard OTF is still limited by $\boldsymbol{k}_{\mathrm{cutoff}} = 2\mathrm{NA}/\lambda$, the incident wavelength will affect our strategy for collecting high-spatial frequency details if we want to avoid "gaps" in our final $\boldsymbol{k}$-space information. Specifically, if we take the approach of following the translation scanning scheme

used in SIM, then the ideal $\boldsymbol{K}$ value would be $2\boldsymbol{k}_{\mathrm{cutoff}}$, since anything higher would result in a region of missing information between our standard OTF and our collected outer lobes. Our nano-antenna array had a pitch corresponding to $2\boldsymbol{k}_{\mathrm{cutoff}}$, which resulted in a tripling of the resolving power compared with standard microscopy, and a doubling of the improvement gained by SIM. Secondly, the nano-antennas have a resonant LP frequency, so exciting them on or off-resonance will affect the strength and features of the LPs. Fig. 2h shows the resonance curve for a single silver nanodisc under normally incident laser illumination. It bears mentioning that a disc presents a different profile to light incident from varied angles, so the localized plasmon spectrum will have some degree of angle dependence. An array of these discs will be subject to additional frequency dependence for a number of reasons, all of which contribute to the final optimized design geometry. For one, constructive interference in the array leads to a sharpening and enhancement of the resonance,[31] and this interference condition changes with the incident angle.[32] Additionally, in a densely packed periodic array, overlap of evanescent fields between adjacent particles can de-phase and reduce the amplitude of the plasmon excitation.[33]

To demonstrate the effectiveness and robustness of the method described above, we tested the performance for the case of a single point particle, a distribution of quantum dots, and a non-sparse object with varying feature sizes. These objects were placed 40 nm behind the back edge of the nano-antenna array, where they were subjected to the near-field patterns generated by the LP excitations. For these simulations, we used fluorescent objects, with an emission wavelength of 430 nm. We assumed that the LP field intensity was in the linear regime of the fluorophore. Furthermore, we assumed that the objects themselves would not dramatically affect the LP fields. The fluorescent emission is controlled by the LP-generated near-field patterns, but to be clear, the actual recorded image is captured in the far field. Near-field, high $\boldsymbol{k}$-value information is decoded and incorporated into the image during the reconstruction post-processing.

Results and discussion

One of the most common ways to characterize the resolution of an imaging technique is with point particles. For this reason, we looked at the full width half maximum (FWHM) and two-point resolution of our technique using 5 nm quantum dots as our object. Shown in Fig. 3a is the standard, diffraction-limited image of a single quantum dot. This is effectively the PSF of the standard system. By comparison, Fig. 3b shows the image (or PSF) using the LPSIM technique. As can readily be observed, there is a marked improvement in resolution. Some asymmetry is introduced, in the form of weak circular artifacts surrounding the central spot. This is a result of an antenna design which maximizes resolution by positioning the high-frequency $\boldsymbol{k}$-space lobes just on the edge of the standard OTF (Fig. 3c). This results in some small gaps in our overall $\boldsymbol{k}$-space information, but it allows us to achieve excellent resolution with only minimal sacrifice in image quality, much of which can be eliminated in post-processing if necessary. Fig. 3d shows a profile across the x-axis of Fig. 3a and b, and from this graph we determine the FWHM. For the standard image, if we assume an oil-immersion NA of 1.4, the FWHM is 153 nm. For the LPSIM image, again with a NA of 1.4, the FWHM is reduced 3-fold to 52 nm. This is a dramatic improvement that surpasses the expected performance of both SIM[34] and metal-dielectric PSIM. No deconvolution is used to enhance this result, although in many relevant specific cases, deconvolution or other numerical processing of the LPSIM image will allow for additional improvement in image quality. It should be noted that some asymmetry is present in our curves due to position-dependent distortion introduced by imperfectly controllable excitation patterns. Another test of resolving power is the Rayleigh criteria.[35] This can be approximated by observing the distance at which two point particles are separated by a 30% intensity dip. As shown in Fig. 3e, two quantum dots spaced 51 nm apart are totally unresolvable with a standard epifluorescence setup. With the LPSIM approach, however, we observe a 30% dip, as expected. This confirms our goal of a 3-fold improvement over the standard image resolution.

While a point particle is useful for measuring FWHM and testing the Rayleigh criteria, many practical objects of interest to biologists and others are more complex. For this reason, we show results for a distribution of many quantum dots, including several that are clustered together. Fig. 4a shows the standard image of such an object, and Fig. 4b shows the LPSIM-recovered object. By normalization of the collected image's frequency-domain magnitude to a generally expected magnitude envelope, a clean, highly resolved image is obtained, shown in Fig. 4c. As can be seen by examination, in addition to a sharpening of single point particles, several unresolved clusters of quantum dots have been resolved into separate points by our LPSIM method. The dot distribution is more general than a single quantum dot, but it is still a sparse object. We also tested a non-sparse converging stripe object (Fig. 4d), which was chosen for its varying feature size as a visual demonstration of resolving power. Fig. 4e and f show the standard and LPSIM images, respectively. Clearly, the diffraction-limited image is completely unresolved in the central region, whereas the LPSIM image reveals the converging stripes deep in towards the center of the object. These objects are shown as examples, but the LPSIM method will be useful for a wide variety of object types.

Like other existing methods, LPSIM has its strengths, but it is not without its disadvantages. Silver as a material choice has drawbacks due to oxidation issues, while gold has a resonance at longer wavelengths, making small geometry arrays inefficient. Although LPSIM is a far-field imaging technique, it relies on near-field LP excitation to induce the fluorescent emission, so any object of interest must be within ~100 nm of the metallic substrate in order for the near-field to have sufficient strength.[36,37] However, this limitation can at times be useful if one wishes to probe only the surface of a sample, without interference from layers at other depths. In a well-designed experiment, quenching and bleaching effects are negligible further than 20 nm from the LP source.[38] In a LPSIM experiment, accurate antenna simulation, fabrication, and alignment

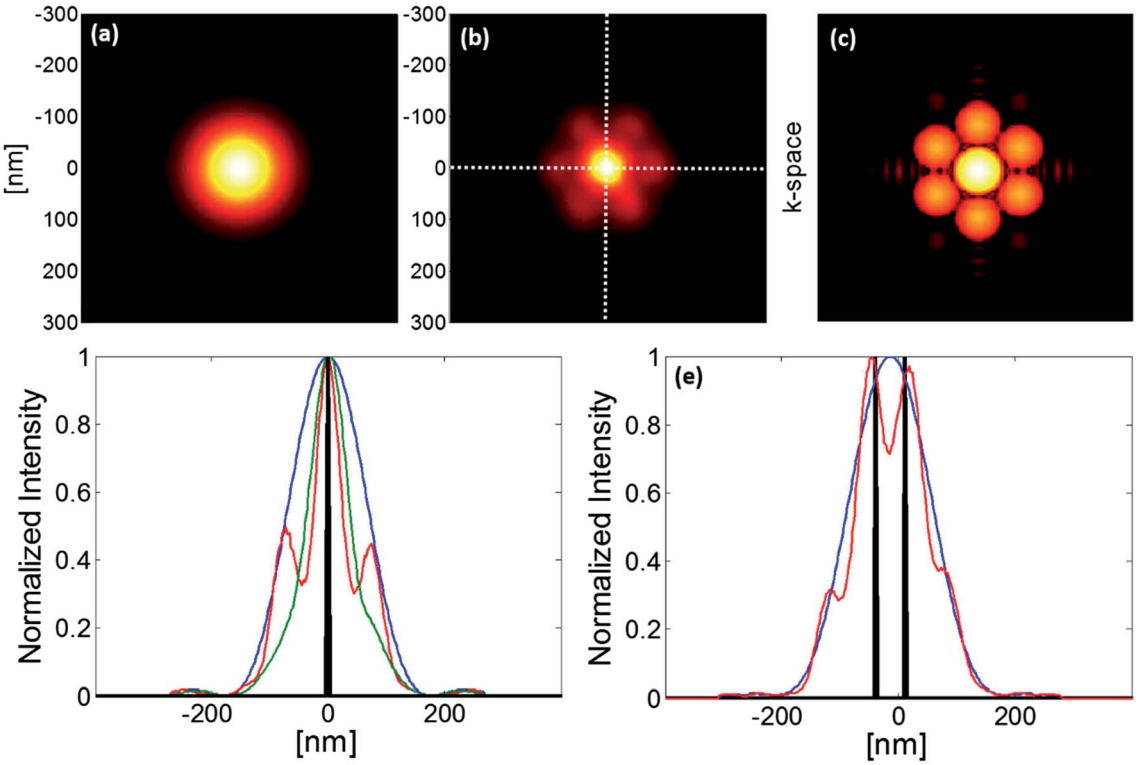

Fig. 3 Resolution characterization: PSFs of (a) a diffraction-limited system, and (b) the LPSIM technique. (c) Expanded OTF after LPSIM reconstruction. Note that the six lobes surrounding the central region are high-frequency information captured by LPSIM. (d) FWHM comparison of diffraction-limited [blue] and LPSIM [red] techniques, for fluorescent emission at 430 nm. The green curve shows the FWHM taken along the vertical line in (b). (e) Two-point resolution. For two 5 nm quantum dots placed 51 nm apart, a standard setup [blue] will not resolve the points, but with LPSIM [red], the typical Rayleigh criteria of a 30% intensity dip is satisfied.

will be important for a reconstruction based on known illumination patterns. Careful design and optimization of the nano-antennas and the incident light polarization is needed, because getting effective pattern translation is difficult with fields confined to a fixed geometry. This limitation in illumination pattern flexibility leads to the irregularities seen in Fig. 4c and f. Fortunately, these problems can be minimized by careful design and reconstruction.

To reiterate, there are a number of advantages to the proposed LPSIM method in comparison with the various existing methods. In point-scanning techniques, if a large field of view relative to the scanning point size is desired, the imaging speed will be slow since the point must scan across the entire plane to reconstruct a single full image. In our method, we translate known, non-sparse excitation patterns in a strategic manner, to collect the information for many locations in parallel, enabling a large field of view without sacrificing speed. Our method is also scalable; for different incident wavelengths the same 3-fold resolution improvement could be achieved by resizing the antennas and the pitch of the array to appropriately position the ***k***-space collection region. The expected imaging speed is similar to that of SIM,[39] with a comparable number of sub-images required to capture each full frame. And to re-emphasize, this method allows us to design illumination patterns with deep sub-wavelength features, regardless of the photonic dispersion curve. The ***k***-space region collected by LPSIM is confined only by fabrication limitations. In fact, in cases such as certain dark-field microscopy setups[40] only very high-***k*** information is relevant. Our method could be used in these situations with even smaller geometry to achieve greater than 3-time resolution improvement. Furthermore, a cleverly designed substrate could be used with multiple feature sizes or a quasi-periodic structure, each excited by a different illumination wavelength. This strategy could be employed to collect information from a larger area in ***k***-space and further enhance resolution. Besides experimental demonstration of this concept, future work could include a combination of PSIM and LPSIM, utilizing the high ***k***-vector of LPSIM in concert with the pattern flexibility of PSIM to make smoother field patterns, allowing for better pattern control. This would allow for high-quality, high-speed, high-resolution imaging. Lastly, designing an antenna with a resonance peak at the incident wavelength enhances fluorescence and reduces the required exposure time.

Conclusions

In conclusion, we have demonstrated a new technique for super resolution imaging, named Localized Plasmon assisted Structured Illumination Microscopy (LPSIM). Our numerical results have shown a resolution improvement larger than that expected from SIM or PSIM, without resorting to high intensity light and the nonlinear response of fluorescence emission subject to such

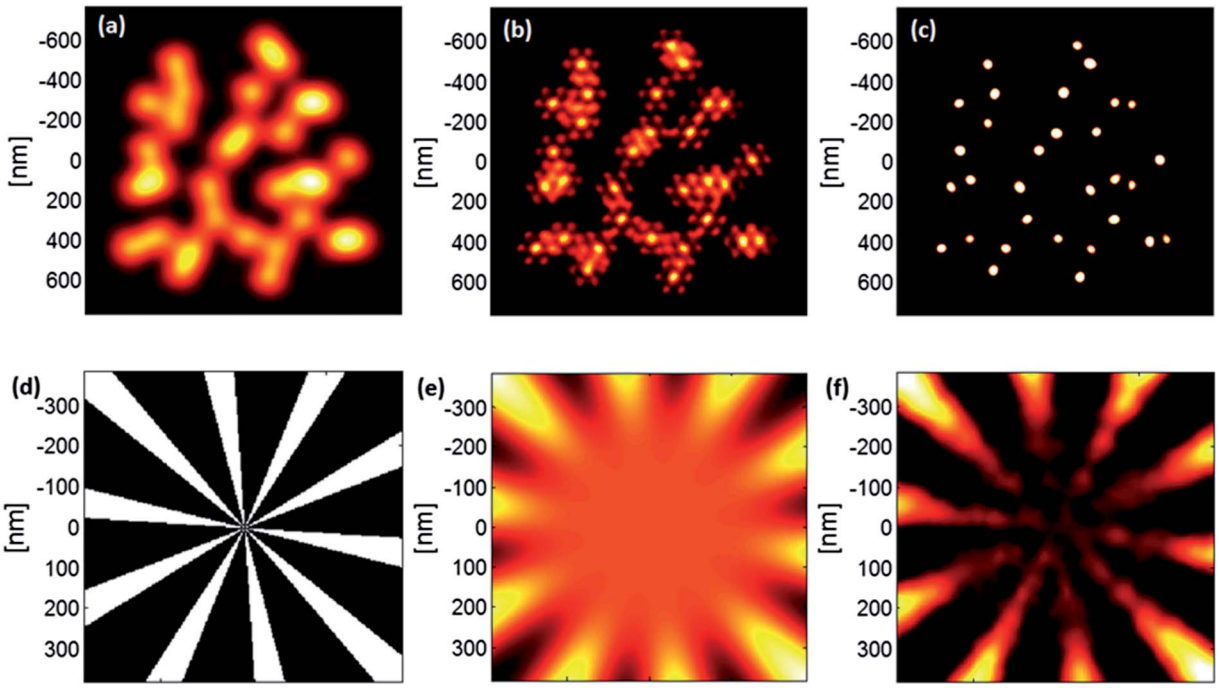

Fig. 4 Imaging results: (a) diffraction-limited image of a distribution of 5 nm-wide fluorescent quantum dots. (b) LPSIM image of the same object. Previously unresolvable points are resolved. (c) Additional Fourier-based deconvolution combined with LPSIM yields a clean, highly resolved image. (d) A solid striped object. (e) Diffraction-limited image. (f) LPSIM image. The stripes are now resolvable much further in towards the center of the image.

light. The objects we have imaged in this paper consistently show a cleanly resolved 3-fold improvement over conventional epifluorescence microscopy. In the future, LPSIM may find useful application in many biological and biomedical fields of research, especially among researchers interested in taking live video of cellular dynamics.

Method

Antenna design and simulation

Our metallic substrate consisted of a hexagonal array of silver disc nano-antennas surrounded by a glass dielectric. The nano-antennas have 60 nm diameter and 60 nm thickness. The pitch is 150 nm. Three-dimensional full-wave CST Microwave Studio frequency domain finite element solver was used to numerically simulate the electromagnetic field distributions in the object plane, with incident light of 405 nm. This excited the nanodiscs at a frequency near their dipole resonance. Ag permittivity was calculated by interpolating data.[41] The imaging calculations were handled analytically, with an Airy pattern PSF.[42]

Illumination scheme

The illumination pattern was recorded in a 2D plane 40 nm behind the nano-antenna array, where we placed our object. Twenty-one sub-images (3 incident planes $\times$ 7 incident angles) were used to fill in our $\boldsymbol{k}$-space picture, as opposed to the typical 9 sub-images (3 pattern orientations $\times$ 3 pattern phases) used in SIM. For high speed imaging, fewer sub-images is preferred, but by adding additional incident angles we were able to improve image quality. The number of sub-images may be decreased with further design optimizations in future work.

Acknowledgements

This research is funded by the Gordon and Betty Moore Foundation.

Notes and references

1 M. J. Rust, M. Bates and X. Zhuang, *Nat. Methods*, 2006, **3**, 793–796.
2 E. Betzig, G. H. Patterson, R. Sougrat, O. W. Lindwasser, S. Olenych, J. S. Bonifacino, M. W. Davidson, J. Lippincott-Schwartz and H. F. Hess, *Science*, 2006, **313**, 1642–1645.
3 S. W. Hell and J. Wichmann, *Opt. Lett.*, 1994, **19**, 780–782.
4 M. Dyba and S. W. Hell, *Phys. Rev. Lett.*, 2002, **88**, 163901.
5 E. A. Ash and G. Nicholls, *Nature*, 1972, **237**, 510–512.
6 D. W. Pohl, W. Denk and M. Lanz, *Appl. Phys. Lett.*, 1984, **44**, 651–653.
7 S. Durant, Z. Liu, J. M. Steele and X. Zhang, *J. Opt. Soc. Am. B*, 2006, **23**, 2383–2392.
8 Z. Liu, S. Durant, H. Lee, Y. Pikus, N. Fang, Y. Xiong, C. Sun and X. Zhang, *Nano Lett.*, 2007, **7**, 403–408.
9 Y. Xiong, Z. Liu, C. Sun and X. Zhang, *Nano Lett.*, 2007, **7**, 3360–3365.
10 A. Salandrino and N. Engheta, *Phys. Rev. B: Condens. Matter Mater. Phys.*, 2006, **74**, 075103.

11 Z. Liu, H. Lee, Y. Xiong, C. Sun and X. Zhang, *Science*, 2007, **315**, 1686.
12 C. Ma and Z. Liu, *Opt. Express*, 2010, **18**, 4838–4844.
13 R. Heintzmann and C. G. Cremer, *Proc. SPIE*, 1999, **3568**, 185–196.
14 J. T. Frohn, H. F. Knapp and A. Stemmer, *Proc. Natl. Acad. Sci. U. S. A.*, 2000, **97**, 7232–7236.
15 L. Schermelleh, P. M. Carlton, S. Haase, L. Shao, L. Winoto, P. Kner, B. Burke, M. C. Cardoso, D. A. Agard, M. G. L. Gustafsson, H. Leonhardt and J. W. Sedat, *Science*, 2008, **320**, 1332–1336.
16 R. Heintzmann, T. M. Jovin and C. Cremer, *J. Opt. Soc. Am. A*, 2002, **19**, 1599–1609.
17 M. G. L. Gustafsson, *Proc. Natl. Acad. Sci. U. S. A.*, 2005, **102**, 13081–13086.
18 F. Wei and Z. Liu, *Nano Lett.*, 2010, **10**, 2531–2536.
19 J. García, Z. Zalevsky and D. Fixler, *Opt. Express*, 2005, **13**, 6073–6078.
20 A. Sentenac, P. C. Chaumet and K. Belkebir, *Phys. Rev. Lett.*, 2006, **97**, 243901.
21 V. Krishnamurthi, B. Bailey and F. Lanni, *Proc. SPIE*, 1996, **2655**, 18–25.
22 E. Mudry, K. Belkebir, J. Girard, J. Savatier, E. L. Moal, C. Nicoletti, M. Allain and A. Sentenac, *Nat. Photonics*, 2012, **6**, 312–315.
23 H. Raether, in *Surface Plasmons on Smooth and Rough Surfaces and on Gratings*, Springer, Berlin Heidelberg, 1988.
24 C. Nylander, B. Liedberg and T. Lind, *Sens. Actuators*, 1983, **3**, 79–88.
25 D. L. Jeanmaire and R. P. V. Duyne, *J. Electroanal. Chem.*, 1977, **84**, 1–20.
26 M. G. Albrecht and J. A. Creighton, *J. Am. Chem. Soc.*, 1977, **99**, 5215–5217.
27 M. Moskovits, *Rev. Mod. Phys.*, 1985, **57**, 783–826.
28 J. Girard, G. Scherrer, A. Cattoni, E. Le Moal, A. Talneau, B. Cluzel, F. de Fornel and A. Sentenac, *Phys. Rev. Lett.*, 2012, **109**, 187404.
29 B. Gjonaj, J. Aulbach, P. M. Johnson, A. P. Mosk, L. Kuipers and A. Lagendijk, *Phys. Rev. Lett.*, 2013, **110**, 266804.
30 S. Liu, C. J. Chuang, C. W. See, G. Zoriniants, W. L. Barnes and M. G. Somekh, *Opt. Lett.*, 2009, **34**, 1255–1257.
31 E. M. Hicks, S. Zou, G. C. Schatz, K. G. Spears, R. P. Van Duyne, L. Gunnarsson, T. Rindzevicius, B. Kasemo and M. Käll, *Nano Lett.*, 2005, **5**, 1065–1070.
32 V. G. Kravets, F. Schedin and A. N. Grigorenko, *Phys. Rev. Lett.*, 2008, **101**, 087403.
33 G. F. Walsh and L. D. Negro, *Nano Lett.*, 2013, **13**, 786–792.
34 M. G. L. Gustafsson, *J. Microsc.*, 2000, **198**, 82–87.
35 A. Wong, in *Resolution Enhancement Techniques in Optical Lithography*, SPIE Press, Bellingham, 2001.
36 W. H. Weber and C. F. Eagen, *Opt. Lett.*, 1979, **4**, 236–238.
37 H. Ditlbacher, J. R. Krenn, N. Felidj, B. Lamprecht, G. Schider, M. Salerno, A. Leitner and F. R. Aussenegg, *Appl. Phys. Lett.*, 2002, **80**, 404–406.
38 W. L. Barnes, *J. Mod. Opt.*, 1998, **45**, 661–699.
39 R. Fiolka, L. Shao, E. H. Rego, M. W. Davidson and M. G. L. Gustafsson, *Proc. Natl. Acad. Sci. U. S. A.*, 2012, **109**, 5311–5315.
40 O. L. Krivanek, M. F. Chisholm, V. Nicolosi, T. J. Pennycook, G. J. Corbin, N. Dellby, M. F. Murfitt, C. S. Own, Z. S. Szilagyi, M. P. Oxley, S. T. Pantelides and S. J. Pennycook, *Nature*, 2010, **464**, 571–574.
41 P. B. Johnson and R. W. Christy, *Phys. Rev. B: Condens. Matter Mater. Phys.*, 1972, **6**, 4370–4379.
42 K. K. Sharma, in *Optics: Principles and Applications*, Academic Press, Burlington, 2006.